Tectonophysics 643 (2015) 44–54

Contents lists available at ScienceDirect

Tectonophysics

journal homepage: www.elsevier.com/locate/tecto

Dating of lithospheric buckling: $^{40}Ar/^{39}Ar$ ages of syn-orocline strike–slip shear zones in northwestern Iberia

Gabriel Gutiérrez-Alonso [a,b,*], Alan S. Collins [c], Javier Fernández-Suárez [d], Daniel Pastor-Galán [a], Emilio González-Clavijo [e], Fred Jourdan [f], Arlo B. Weil [g], Stephen T. Johnston [h]

[a] Departamento de Geología, Universidad de Salamanca, 37008 Salamanca, Spain
[b] Geology and Geography Department, Tomsk State University, Lenin Street 36, Tomsk 634050, Russian Federation
[c] Tectonics, Resources and Exploration (TRaX), Department of Earth Sciences, University of Adelaide, SA 5005, Australia
[d] Departamento de Petrología y Geoquímica, Universidad Complutense, IGEO, CSIC, 28040 Madrid, Spain
[e] IGME, Unidad de Salamanca, C/Azafranal, 48, 37001 Salamanca, Spain
[f] Western Australian Argon Isotope Facility, Dept of Applied Geology and JdL Centre, Curtin University, GPO Box U1987, Perth, WA 6845, Australia
[g] Department of Geology, Bryn Mawr College, Bryn Mawr, PA 19010, USA
[h] School of Earth & Ocean Sciences, University of Victoria, PO Box 3065 STN CSC, Victoria, BC V8P 4B2, Canada

ARTICLE INFO

Article history:
Received 17 June 2014
Received in revised form 22 December 2014
Accepted 24 December 2014
Available online 7 January 2015

Keywords:
Ar–Ar geochronology
Orocline
Iberia
Shear zones

ABSTRACT

Orogenic curvature is a ubiquitous feature of mountain belts, and the plate tectonic and geodynamic setting responsible for the development of curved orogens is a subject of debate. In order to distinguish between different models of orocline formation it is necessary to tightly constrain the absolute timing of oroclinal development. However, determining the absolute (isotopic) timing of oroclinal bending is challenging. The most direct method available to constrain the time interval during which an orocline formed is to obtain absolute age constraints on fabrics generated within syn-orocline strike–slip shear zones that accommodated rotations around a vertical axis during the development of crustal or lithospheric scale orogenic curvature. Here we present a data set of $^{40}Ar/^{39}Ar$ ages obtained from five shear-zones, some of which display curved traces parallel to the Cantabrian Orocline structural grain in NW Iberia and are interpreted to have been generated coevally to it. The $^{40}Ar/^{39}Ar$ ages were obtained by laser-rastering induced step-heating on single muscovite crystals that grew synkinematically during shearing. All five samples yielded ages that cluster tightly at 308 ± 3 Ma providing direct evidence for the age of oroclinal bending. This age is consistent with the age constraints obtained from paleomagnetic and structural data that place the onset of oroclinal bending in Moscovian times. Our $^{40}Ar/^{39}Ar$ age determinations therefore provide a reliable absolute constraint on the age of buckling of the Variscan orogen around a vertical axis and provide further evidence that oroclinal bending is unrelated to Variscan convergence/collision or the subsequent extensional collapse of the mountain belt.

1. Introduction

Oroclines are drawing increasing scientific attention driven by the realization that they are widespread in mountain belts and involve the whole lithosphere (e.g. Johnston et al., 2013 and references therein). As a consequence, unraveling the kinematics and chronology of an orocline is an essential first step in understanding a curved orogen and its attendant tectonic evolution and significance. Curved mountain belts have been identified world-wide and their genetic relation to plate tectonic processes remains controversial (see Gutiérrez-Alonso et al., 2004, 2008; Johnston et al., 2013; Maffione et al., 2009, 2010, 2013; Marshak, 2004; Rosenbaum et al., 2012; Van der Voo, 2004; Weil et al., 2010, 2013). Arguably the most studied curved orogenic system is that formed by the coupled oroclines of the West European Variscan Belt (WEVB) that form the Iberian–Armorican Arc (Argand, 1924; Bard et al., 1968; Carey, 1955) including the Cantabrian Arc or Orocline (Gutiérrez-Alonso et al., 2012; Weil et al., 2013) and the Central Iberian Arc or Orocline (Aerden, 2004; Martínez-Catalán, 2011, 2012; Shaw et al., 2012) (Fig. 1A).

The origin, timing and kinematic development of the Cantabrian Arc as a lithospheric-scale buckle, has been discussed over the past 25 years and many hypotheses and models have been proposed to explain its curvature as having formed prior to (e.g. Arthaud and Matte, 1977; Ribeiro et al., 2007) or coeval with Variscan orogenic development (e.g. Kröner and Romer, 2013; Martínez Catalán et al., 2007; Martínez-Catalán, 1990; Martínez-García, 2013; Şengör, 2013; Simancas et al., 2005, 2013) or postdating it (e.g. Gutiérrez-Alonso et al., 2004, 2008; Martínez-Catalán, 2011, 2012; Pastor-Galán et al.,

* Corresponding author at: Department, Salamanca university, 37008, Salamanca, Spain and Tomsk State University, Tomsk, Russia.
E-mail address: gabi@usal.es (G. Gutiérrez-Alonso).

http://dx.doi.org/10.1016/j.tecto.2014.12.009
0040-1951/

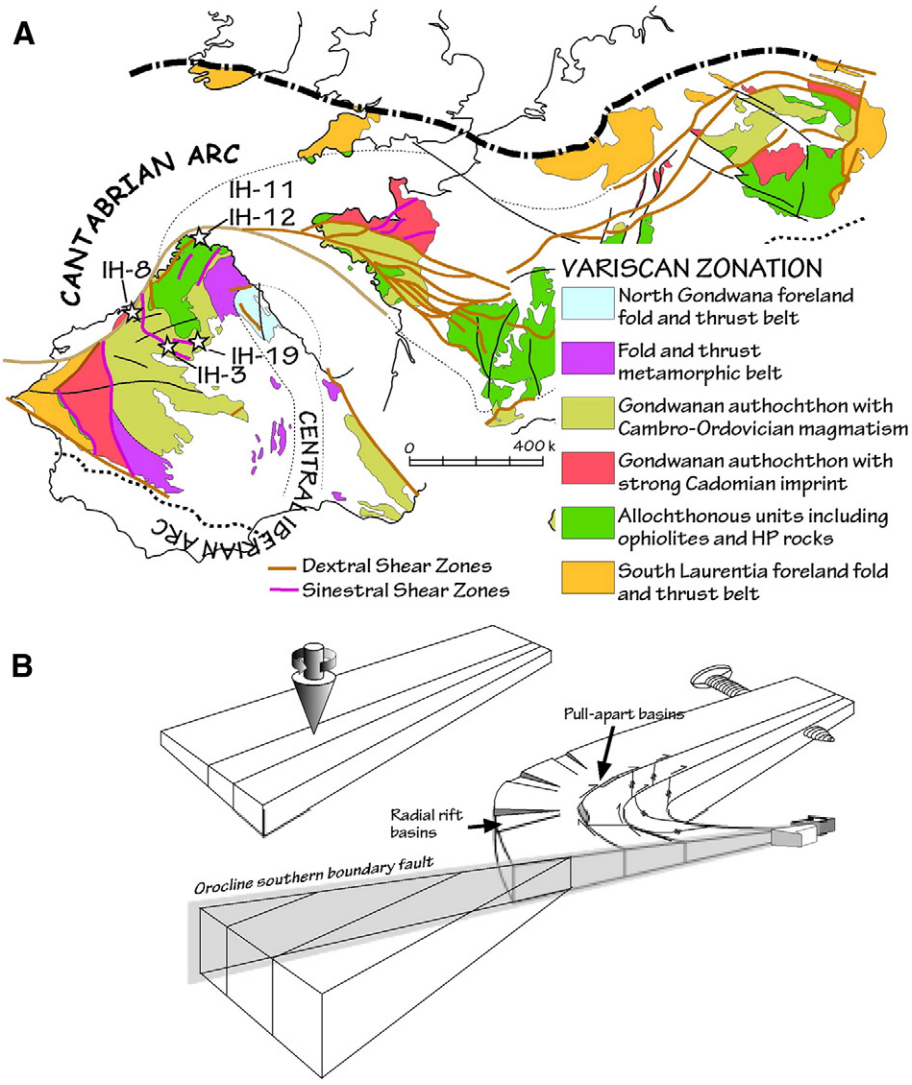

Fig. 1. (A) Main architecture of the Iberian–Armorican Arc in the West European Variscan Belt depicting the major Late-Variscan strike–slip shear zones studied in this paper. Stars indicate the sampling locations described in the text. Figure modified from Martínez-Catalán (2011) and Shaw et al. (2012). (B) Conceptual model of shear zone generation during oroclinal buckling (Gutiérrez-Alonso et al., 2008).

2011; Shaw et al., 2012; Weil et al., 2001, 2013). Extensive paleomagnetic data constrain the orocline development to uppermost Carboniferous times (from Moscovian to latest Gzhelian times; ~310–299 Ma) (Van der Voo et al., 1997; Weil et al., 2000, 2001, 2010, 2013). Additionally, chronologically constrained structural data have been used to constrain the relative timing of buckling in the Cantabrian Arc, including calcite twin analysis by Kollmeier et al. (2000), and fracture analysis by Pastor-Galán et al. (2011). However, all of these studies rely on the assumed relative timing of magnetization acquisition, or the age of syn-tectonic sediment deposition for bracketing the age and extent of oroclinal buckling. This approach could only be performed in the core of the Cantabrian Arc, as it is the only place where suitable rocks for this kind of analysis have been found. Other studies have dated intrusive rocks to constrain the age of other geological phenomena interpreted to be related to orocline formation (see ahead).

In order to provide absolute age constraints on the timing of deformation, and to link the evolution of the external part of the arc with the better constrained kinematics of its core, we have undertaken a $^{40}Ar/^{39}Ar$ geochronologic study of a large-scale strike–slip shear zone system that is interpreted to have accommodated lithospheric scale oroclinal bending at the mid- to upper-crustal levels (Fig. 1). The $^{40}Ar/^{39}Ar$ chronometric data presented here, as well as existing geochronologic and structural data from other large scale strike–slip faults from the WEVB (e.g. Ballèvre et al., 2009; Le Carlier de Veslud et al., 2013; Tartese et al., 2011; Turrillot et al., 2011), are consistent with the strike–slip shear zones having been active during orocline formation as constrained by existing structural and paleomagnetic studies, and strengthen the interpretation of the Cantabrian Arc as a secondary orocline (Carey, 1955; Johnston et al., 2013; Weil and Sussman, 2004).

2. Geological background

The WEVB is part of the mostly Carboniferous orogenic system that extends from Central Europe (Variscan) into North America (Appalachians and Ouachitas) and northwest Africa (Mauritanides). The origin and evolution of the WEVB in Iberia is well constrained and includes building of the orogenic architecture in a time span of ~45 Ma, from initial subduction of the Gondwanan passive margin at ~365 Ma to extensional collapse of the main orogen at ~320 Ma (e.g. Costa et al., 2014; Díez Balda et al., 1995; Martínez Catalán et al., 2007; Pereira et al., 2009, 2012; Simancas et al., 2005). Questions remain regarding the subsequent tectonic modification of the belt that took place in Late Pennsylvanian and earliest Permian times, commonly referred to as "Late Variscan". The so called Late Variscan is not commonly

interpreted as a major tectonic event, despite this time interval being characterized by the following: a) voluminous magmatism across the entire orogen, including the foreland (Fernández-Suárez et al., 2000; Gutiérrez-Alonso et al., 2011a; Orejana et al., 2012 and references therein); b) low-P/high-T metamorphism (e.g. Arenas and Martínez Catalán, 2003; Buck et al., 1988; Fernández Suárez, 1994; Martínez and Rolet, 1988); c) widespread genesis of Au, Sb–Hg, and W–Sn mineral deposits (e.g. Cepedal et al., 2013; Martín-Izard et al., 2000, 2009); d) extensive partial melting and HT metamorphism of the lower crust (Fernandez-Suarez et al., 2006; Orejana et al., 2011); e) buckling of the Cantabrian Arc (Weil et al., 2001, 2010, 2013); f) lithospheric mantle replacement (Gutiérrez-Alonso et al., 2011b; Pereira et al., 2012, in press); and g) a complex array of sub-vertical strike–slip shear zones with abundant well-preserved mylonites and other shear-related fabrics. This study focuses on the chronology of Late Variscan shear zones in the context of a model of regional oroclinal buckling that involves the entire lithosphere (see Gutiérrez-Alonso et al., 2004, 2012; Weil et al., 2013 and Johnston et al., 2013 for a summary the oroclinal lithospheric models).

The geologic framework of the WEVB is dominated by the curved geometry of the main crustal structures (e.g., traces of thrusts, fold axial plane traces and extensional detachments) previously formed during the continental collision that attended the closure of the Rheic Ocean (Fig. 1) and subsequent intra-orogenic extension. In northern Iberia the main structures of the Cantabrian Arc trend E–W to NNE–SSW, intersecting the Cantabrian Sea coastline, whereas in central Iberia the structures rotate progressively towards a WNW–ESE orientation. The Late Variscan shear-zones overprint the main structural grain, and form a similar, but more open, curved pattern. Dextral strike–slip shear zones are predominantly sub-parallel to the main Variscan structures, although the most prominent one (the N–S trending Porto-Tomar shear zone) is oblique to them. In contrast, most of the sinistral shear zones are oriented oblique to the main structural grain (Fig. 1A). These shear zones have been variously interpreted as follows: 1) part of a major dextral shear zone between the Appalachians and the Urals (Arthaud and Matte, 1977); 2) the result of a corner effect during continental collision (Brun and Burg, 1982); 3) escape structures around a rigid indenter, which is inferred to form the core of the Cantabrian Arc (Dias and Ribeiro, 1995; Ribeiro et al., 2007); 4) a response to a N–S compressive stress field (Marques et al., 2002); 5) large-scale structures that accommodated oblique (dextral) convergence between Gondwana and Laurussia (Martínez-Catalán, 2011; Shelley and Bossière, 2002); and finally 6) the result of dominantly dextral shear and less pervasive conjugate sinistral shearing attributable to the oroclinal buckling that gave rise to the Cantabrian Arc (Fig. 1B) (Gutiérrez-Alonso et al., 2004, 2008).

Individual greenschist-facies shear zones within the larger WEVB shear zone system (Fig. 1B) preserve a pervasive foliation that overprints previously deformed and metamorphosed sedimentary and igneous rocks producing phyllonites and mylonites that are commonly characterized by well developed S–C fabrics. All the shear zones in this study are characterized by syn-kinematic muscovite, which in most cases formed at the expense of magmatic biotite or biotite that had developed during earlier regional metamorphic events. Quartz c-axis studies in some shear zones (González-Clavijo, 1990) reveal low to medium temperature conditions (350–400 °C) during shear zone development. All shear zones are characterized by the presence of abundant kinematic indicators (see representative microphotographs in Fig. 2).

The relative timing of major WEVB strike–slip shear zones was previously constrained to ca. 315–295 Ma using structural relations with granitoid plutons of known age that were either deformed by the shear zones or cut cross them (Aguado et al., 2005; Gutiérrez-Alonso et al., 2011a,b; Martins. et al., 2011; Pereira et al., 2010; Valverde-Vaquero et al., 2007) although the age constraints were not linked to the orocline formation.

3. Sampling and analytical procedures

For this study, samples were collected from within five of the main ductile shear zones of NW Iberia, in rocks with pervasive sub-horizontal lineation and sub-vertical shear-mylonitic related foliation. Sampling was focused on those rocks in which muscovite grew in the foliation planes syn-kinematically with strike–slip shear deformation (Fig. 2) or strongly deformed and retrogressed as mica-fish (Lister and Snoke, 1984). All the studied samples were chosen after detailed screening using thin sections where the nature of the white micas in the foliation planes could be established as syn-kinematic. Examples of representative thin section microphotographs from surfaces normal to shear foliation and parallel to the stretching lineation are shown in Fig. 2. Most of the syn-kinematic muscovite grains are attributable to retrogression of biotite grains during shear development, intense deformation of previous muscovite large grains and/or muscovite porphyroblast growth.

Five fresh samples, representative of the main ductile shear zones (location in Fig. 1, coordinates in the sample description section) were selected for $^{40}Ar/^{39}Ar$ dating. Unaltered, optically transparent, 200–1000 μm-size muscovite grains were separated from these samples and those selected for analysis were hand-picked under a binocular microscope and thoroughly rinsed with distilled water in an ultrasonic cleaner.

The samples were loaded into 5 large wells of a 1.9 cm diameter and 0.3 cm depth aluminium disc. The Hb3gr hornblende standard was used as a neutron fluence monitor, for which an age of 1074 ± 4 Ma was adopted at the time of the measurement and a good in-between grain reproducibility has been demonstrated (Jourdan et al., 2006). The discs were Cd-shielded (to minimize undesirable nuclear interference reactions) and irradiated for 30 h in the Hamilton McMaster University nuclear reactor (Canada) in position 5C. The weighted-mean J-value computed from standard grains within the small pits is 0.010622 ± 0.000042 (0.40%). Mass discrimination was monitored using an automated air pipette and provided values ranging from 0.9986 ± 0.0032 to 1.0018 ± 0.0042 per Dalton (atomic mass unit). The correction factors for interfering isotopes were $(^{39}Ar/^{37}Ar)_{Ca} = 7.30 \times 10^{-4}$ (±11%), $(^{36}Ar/^{37}Ar)_{Ca} = 2.82 \times 10^{-4}$ (±1%) and $(^{40}Ar/^{39}Ar)_{K} = 6.76 \times 10^{-4}$ (±32%).

The $^{40}Ar/^{39}Ar$ analyses were performed at the Western Australian Argon Isotope Facility at Curtin University, operated by a consortium consisting of Curtin University and the University of Western Australia. Each sample was run using a single-grain of muscovite. The samples were step-heated using a 110 W Spectron Laser Systems, with a continuous Nd-YAG (IR; 1064 nm) laser rastered over the sample during 1 min to ensure a homogenously distributed temperature. The gas was purified in a stainless steel extraction line using a GP50 and two AP10 SAES getters. Argon isotopes were measured in static mode using a MAP 215-50 mass spectrometer (resolution of ~600; sensitivity of 2×10^{-14} mol/V) with a Balzers SEV 217 electron multiplier mostly using 9 to 10 cycles of peak-hopping. The data acquisition was performed with the Argus program written by M.O. McWilliams and ran under a LabView environment. The raw data were processed using the ArArCALC software (Koppers, 2002) and the ages have been calculated using the decay constants recommended by Steiger and Jäger (1977). Blanks were monitored every 3 to 4 steps and typical ^{40}Ar blanks range from 1×10^{-16} to 2×10^{-16} mol. Ar isotopic data and errors corrected for blank, mass discrimination and radioactive decay are given in Tables 1–5 at the 1σ level. Our criteria for the determination

Fig. 2. Photomicrographs of the studied samples of mylonites. All thin sections were cut normal to the shear foliation and parallel to the stretching lineation observable in the rocks. For all samples shear foliation is defined by muscovite and abundant kinematic criteria (mica-fish, S–C fabrics, etc.) can be observed.


1000 μm
IH-03
1000 μm
Juzbado-Traguntia-Penalva do Castelo Shear Zone
IH-03
500 μm
IH-08
500 μm
Porto-Tomar Shear Zone
IH-08
500 μm
IH-11
500 μm
Malpica-Lamego Shear Zone
IH-11
1000 μm
IH-12
1000 μm
Punta Langosteira Shear Zone
IH-12
1000 μm
IH-19
1000 μm
Villalcampo Shear Zone
IH-19

Table 1
Sample IH-03.
This table includes the laser power, the relative abundances of all argon isotopes, the percentage of radiogenic ^{40}Ar, the percentage of ^{39}Ar and the individual apparent ages for each step. Plateau ages are given for each sample, below. Note that all ages have been measured with the constants of Steiger and Jäger (1977). Plateau ages recalculated with a new set of decay constants proposed by Renne et al. (2010) are given in the text and in Fig. 3 which shift all apparent ages by +1%. Laser intensity intervals with * have not been used for the plateau age calculations.

Laser intensity (%)	$^{36}Ar \pm 1\sigma$		$^{37}Ar \pm 1\sigma$		$^{38}Ar \pm 1\sigma$		$^{39}Ar \pm 1\sigma$		$^{40}Ar \pm 1\sigma$		$^{40}Ar^*$ (%)	$^{39}Ar_K$ (%)	Age ± 2σ (Ma)	
IH-3			J = 0.0106220 ± 0.0000425											
56.20W*	0.000086	0.000003	0.000237	0.000013	0.000038	0.000002	0.000512	0.000007	0.014250	0.000066	79.53	0.23	268.84	±81.88
56.50W*	0.000082	0.000003	0.000248	0.000011	0.000031	0.000002	0.000608	0.000003	0.015882	0.000071	94.51	0.27	310.24	±69.74
57.20W*	0.000094	0.000006	0.000280	0.000007	0.000079	0.000005	0.004013	0.000028	0.075077	0.000158	93.74	1.81	290.52	±16.26
57.50W	0.000084	0.000005	0.000267	0.000013	0.000051	0.000004	0.001789	0.000013	0.036742	0.000116	96.18	0.80	304.16	±34.17
57.80W	0.000090	0.000006	0.000250	0.000009	0.000054	0.000004	0.001912	0.000008	0.038277	0.000100	96.55	0.86	299.00	±34.42
58.20W	0.000082	0.000003	0.000275	0.000011	0.000057	0.000005	0.002890	0.000026	0.055408	0.000144	100.00	1.30	308.18	±5.77
58.50W	0.000085	0.000005	0.000277	0.000008	0.000118	0.000003	0.008278	0.000042	0.149310	0.000248	100.00	3.74	306.62	±3.52
58.60W	0.000082	0.000003	0.000250	0.000012	0.000083	0.000006	0.005003	0.000036	0.091715	0.000146	100.00	2.26	305.46	±4.52
58.70W	0.000088	0.000005	0.000225	0.000011	0.000070	0.000002	0.004376	0.000035	0.080053	0.000137	97.78	1.98	296.70	±17.05
59.20W	0.000085	0.000003	0.000296	0.000013	0.000076	0.000005	0.003931	0.000019	0.073641	0.000197	99.04	1.77	305.39	±16.03
59.50W	0.000090	0.000003	0.000298	0.000007	0.000125	0.000005	0.008208	0.000045	0.148845	0.000232	98.49	3.71	303.93	±8.42
59.70W	0.000081	0.000004	0.000238	0.000017	0.000140	0.000006	0.008654	0.000031	0.157538	0.000150	100.00	3.91	309.76	±2.83
60.00W	0.000080	0.000003	0.000241	0.000008	0.000292	0.000009	0.021411	0.000069	0.380228	0.000492	100.00	9.69	307.65	±2.69
60.20W	0.000077	0.000004	0.000225	0.000008	0.000607	0.000013	0.049105	0.000133	0.860364	0.000966	100.00	22.23	305.78	±2.44
60.10W	0.000092	0.000003	0.000283	0.000009	0.000414	0.000005	0.031192	0.000110	0.552103	0.000561	99.53	14.12	306.48	±3.41
60.50W	0.000078	0.000003	0.000312	0.000011	0.000132	0.000007	0.009334	0.000079	0.169949	0.000401	100.00	4.22	310.37	±5.39
61.00W	0.000087	0.000004	0.000297	0.000007	0.000176	0.000009	0.011559	0.000035	0.205079	0.000262	99.47	5.23	302.93	±6.42
62.00W	0.000082	0.000003	0.000274	0.000012	0.000384	0.000005	0.029986	0.000106	0.528985	0.000392	100.00	13.58	306.72	±2.73
65.00W	0.000086	0.000004	0.000258	0.000009	0.000242	0.000008	0.018291	0.000074	0.327457	0.000374	99.77	8.28	308.69	±4.64

Results	40(r)/39(k)	±2σ	Age (Ma)	±2σ	MSWD	$^{39}Ar(k)$ (%,n)	K/Ca	±2σ
Weighted Plateau	17.4694	±0.0638 ±0.37%	307.08	±2.48 ±0.81%	0.79	97.70 16	0.517	±1.185
			External Error	±2.72	2.13	Statistical T Ratio		
			Analytical Error	±1.03	1.0000	Error Magnification		
Total Fusion Age	17.4033	±0.0805 ±0.46%	306.01	±2.60 ±0.85%		19	67.039	±94.872
			External Error	±2.82				
			Analytical Error	±1.30				

of plateaus are as follows: plateaus must include at least 70% of ^{39}Ar. The plateau should be distributed over a minimum of 3 consecutive steps agreeing at 95% confidence level and satisfying a probability of fit (P) of at least 0.05. Plateau ages (Tables 1–5 and Fig. 3) are given at the 2σ level and are calculated using the mean of all the plateau steps, each weighted by the inverse variance of their individual analytical error. Integrated ages (2σ) are calculated using the total gas released for each Ar isotope. Inverse isochrons include the maximum number of steps with a probability of fit of ≥0.05. All the plateau ages have been recalculated using the decay constant of Renne et al. (2010) and the $R_{FCs/Hb3gr}$ value of Jourdan and Renne (2007). All sources of uncertainty are included in the calculation and have been calculated using the optimization method of Renne et al. (2010).

4. Sample description

4.1. The Juzbado–Traguntia–Penalva do Castelo Shear Zone (Iglesias and Ribeiro, 1981)

Sample IH-3 (40°57′35.20″N–6°21′51.36″W) was collected from a sinistral ductile shear zone that can be traced for more than 200 km, is up to 4 km wide and trends ENE–WSW (Figs. 1 and 4C) This sinistral ductile shear zone displaces previous folded extensional shear zones (Villar Alonso et al., 1992). The sampled rock is an intensely strained, coarse-grained mylonite developed in a leucogranite (Moronta granite) with S–C fabric (Fig. 2). The white mica grains that were picked for analysis were 300–800 μm in diameter, and were found on the C-planes in a S–C mylonite. S–C fabrics and abundant "mica fish" structures (Fig. 2) provide unequivocal left-lateral shear sense indicators. The inferred displacement across this shear zone is ~100 km (Villar Alonso et al., 1992). A previous K–Ar age of micas from a foliation plane linked to the shear fabric yielded an age of 302 ± 6 Ma (Regencio Macedo, 1988). U–Pb geochronological data in granites post-dating the formation of this shear zone have provided ages of 304 ± 3, 300 ± 3 Ma (Villavieja de Yeltes and Cipérez granites respectively, Gutiérrez-Alonso et al., 2011a,b) and 303 ± 8 (Aguiar de Beira granites, Costa, 2011).

4.2. The Porto-Tomar shear zone (PTSZ) (Ribeiro et al., 1980)

Sample IH-8 (40°54′13.54″N–8°29′2.04″W) was collected from an intensely foliated medium-grained muscovite-rich mylonitic felsic schist (phyllonite) (Fig. 2). The mylonitic foliation is defined mostly by muscovite, which was used to obtain the age in this study. The white mica grains that were picked for analysis were 200–500 μm in diameter. Sparse quartz and feldspar porphyroclasts provide dextral kinematic criteria. This shear zone cuts across most of western Iberia around the outside of the Cantabrian Arc, and is interpreted to continue into the South Armorican Shear Zone of France (Shelley and Bossière, 2002). In western Iberia this shear zone trends close to N–S (Figs. 1B and 4C) and displaces one of the main WEVB paleogeographic boundaries, the Central Iberian — Ossa–Morena Zone limit (Fig. 1A and B). The 2 to 8 km wide shear zone affects low-grade rocks that show abundant dextral kinematic indicators, and is characterized by >170 km of dextral displacement. The origin of the PTSZ has been a subject of intense debate owing to the postulation of a protracted evolution throughout most of the Paleozoic (e.g. Martínez-Catalán, 1990; Ribeiro et al., 2007; Shelley and Bossiere, 2000; Simancas et al., 2005). However,

Table 2
Sample IH-08.
Same caption as in Table 1.

Laser intensity (%)	$^{36}Ar \pm 1\sigma$		$^{37}Ar \pm 1\sigma$		$^{38}Ar \pm 1\sigma$		$^{39}Ar \pm 1\sigma$		$^{40}Ar \pm 1\sigma$		$^{40}Ar^*$(%)	$^{39}Ar_K$ (%)	Age $\pm 2\sigma$ (Ma)	
IH-08					J = 0.0106220 ± 0.0000425									
56.20W	0.000080	0.000005	0.000163	0.000011	0.000038	0.000003	0.001309	0.000009	0.027640	0.000065	83.17	9.29	12.555	±162.975
56.40W	0.000076	0.000004	0.000172	0.000011	0.000137	0.000006	0.010071	0.000037	0.180371	0.000116	98.57	71.77	12.941	±21.044
67.00W	0.000056	0.000007	0.000116	0.000011	0.000050	0.000003	0.002662	0.000024	0.050605	0.000137	100.00	18.94	12.941	±21.044

Results	40(r)/39(k)	±2σ	Age (Ma)	±2σ	MSWD	$^{39}Ar(k)$ (%,n)	K/Ca	±2σ
Weighted Plateau	17.4694	±0.0638 ±0.37%	305.32	±5.72 ±1.87%	1.55	100.00 3	12.938	±14.919
			External Error	±5.82	4.30	Statistical T Ratio		
			Analytical Error	±5.26	1.2456	Error Magnification		
Total Fusion Age	17.0425	±0.4455 ±2.61%	300.17	±7.56 ±2.52%		3	15.909	±40.408
			External Error	±7.64				
			Analytical Error	±7.23				

this contention is not supported by recently published U–Pb data (Pereira et al., 2010) or our geochronological data (see below).

4.3. The Malpica–Lamego Shear Zone (*Ponce de Leon and Choukroune, 1980*)

Sample IH-11 (43°19′48.23″N–8°49′43.87″W) was collected from a medium-grained muscovite-biotite mylonitic schist (Fig. 2). The white mica grains that were picked for analysis were 500–900 μm in diameter "mica fish" structures, quartz aggregates and sparse feldspar porphyroclasts provide dextral kinematic indicators. The shear zone has a curved trajectory that parallels the Cantabrian Arc and extends for more than 275 km along strike, and is characterized by a minimum dextral displacement of 28 km (Llana-Funez and Marcos, 2001). Previous $^{40}Ar/^{39}Ar$ ages of 303 ± 6 and 308 ± 6 Ma were obtained from two samples (Rodriguez et al., 2003) in syn-kinematic granitoids within the studied shear zone. The dextral shear zone has been interpreted to have reactivated a pre-existing crustal-scale thrust (Llana-Funez and Marcos, 2001) that developed during the main Variscan collisional event (Díez Fernández et al., 2011).

4.4. The Punta Langosteira Shear Zone (*Díaz García, 1990*)

Sample IH-12 (43°21′15.07″N–8°29′19.56″W) is a fine-grained quartz-feldspar S–C mylonite with abundant "mica fish" structures and feldspar porphyroclasts that indicate a dextral shear sense (Fig. 2). The white mica grains that were picked for analysis were 600–1000 μm in diameter. The sample was collected from an intensely strained felsic granite. Overall, the shear zone trends N30°E, displays dextral sense of shear, and has accommodated kilometre-scale

Table 3
Sample IH-11.
Same caption as in Table 1.

Laser intensity (%)	$^{36}Ar \pm 1\sigma$		$^{37}Ar \pm 1\sigma$		$^{38}Ar \pm 1\sigma$		$^{39}Ar \pm 1\sigma$		$^{40}Ar \pm 1\sigma$		$^{40}Ar^*$ (%)	$^{39}Ar_K$ (%)	Age $\pm 2\sigma$ (Ma)	
IH-11					J = 0.0106220 ± 0.0000425									
55.70W	0.000068	0.000005	0.000180	0.000022	0.000020	0.000005	0.000006	0.000003	0.004116	0.000158	98.94	2.63	317.70	±45.81
56.00W	0.000068	0.000005	0.000177	0.000022	0.000020	0.000005	0.000006	0.000003	0.004109	0.000158	97.72	7.20	311.88	±19.37
56.00W	0.000068	0.000005	0.000174	0.000022	0.000020	0.000005	0.000007	0.000003	0.004105	0.000158	98.04	6.38	316.55	±23.51
56.30W	0.000067	0.000005	0.000171	0.000022	0.000019	0.000005	0.000007	0.000003	0.004098	0.000158	99.28	14.10	308.18	±11.17
56.30W	0.000066	0.000005	0.000167	0.000022	0.000019	0.000005	0.000008	0.000003	0.004089	0.000158	100.00	14.51	309.64	±3.35
56.40W	0.000066	0.000005	0.000165	0.000022	0.000019	0.000005	0.000009	0.000003	0.004084	0.000158	100.00	10.13	311.96	±4.84
56.50W	0.000066	0.000005	0.000163	0.000022	0.000019	0.000005	0.000009	0.000003	0.004080	0.000158	96.70	6.26	304.04	±26.07
56.60W	0.000065	0.000005	0.000161	0.000022	0.000019	0.000005	0.000010	0.000003	0.004076	0.000158	93.90	3.84	287.68	±34.39
56.70W	0.000065	0.000005	0.000158	0.000022	0.000019	0.000005	0.000010	0.000003	0.004071	0.000158	99.38	6.19	308.06	±21.23
56.80W	0.000070	0.000007	0.000182	0.000055	0.000020	0.000005	0.000007	0.000003	0.004111	0.000055	100.00	2.43	314.87	±8.12
57.10W	0.000071	0.000007	0.000184	0.000055	0.000020	0.000005	0.000005	0.000003	0.004106	0.000055	97.57	2.79	299.30	±62.36
57.60W	0.000071	0.000007	0.000187	0.000055	0.000020	0.000005	0.000003	0.000003	0.004096	0.000055	100.00	2.48	299.84	±5.43
57.80W	0.000072	0.000007	0.000189	0.000055	0.000021	0.000005	0.000002	0.000003	0.004087	0.000055	89.83	3.15	280.22	±52.74
58.40W	0.000073	0.000007	0.000194	0.000055	0.000021	0.000005	0.000001	0.000003	0.004060	0.000055	100.00	3.25	309.23	±7.48
58.60W	0.000073	0.000007	0.000197	0.000055	0.000022	0.000005	0.000001	0.000003	0.004044	0.000055	99.08	3.56	300.83	±55.22
59.50W	0.000074	0.000007	0.000200	0.000055	0.000022	0.000005	0.000002	0.000003	0.004021	0.000055	100.00	2.27	310.82	±8.89
63.60W	0.000074	0.000007	0.000203	0.000055	0.000022	0.000005	0.000004	0.000003	0.003993	0.000055	100.00	8.82	305.07	±4.77

Results	40(r)/39(k)	±2σ	Age (Ma)	±2σ	MSWD	$^{39}Ar(k)$ (%,n)	K/Ca	±2σ
Weighted Plateau	17.5401	±0.1361 ±0.78%	308.22	±3.16 ±1.02%	1.32	100.00 17	0.772	±0.601
			External Error	±3.35	2.12	Statistical T Ratio		
			Analytical Error	±2.20	1.1504	Error Magnification		
Total Fusion Age	17.4750	±0.3069 ±1.76%	307.17	±5.45 ±1.77%		17	8.514	±20.373
			External Error	±5.56				
			Analytical Error	±4.96				

Table 4
Sample IH-12.
Same caption as in Table 1.

Laser intensity (%)	$^{36}Ar \pm 1\sigma$		$^{37}Ar \pm 1\sigma$		$^{38}Ar \pm 1\sigma$		$^{39}Ar \pm 1\sigma$		$^{40}Ar \pm 1\sigma$		$^{40}Ar^{*}$ (%)	$^{39}Ar_K$ (%)	Age $\pm 2\sigma$ (Ma)	
IH-12	J = 0.0106220 ± 0.0000425													
57.50W	0.000091	0.000004	0.000220	0.000011	0.000139	0.000005	0.009338	0.000038	0.167813	0.000261	98.00	8.86	301.79	±5.88
57.80W	0.000080	0.000004	0.000112	0.000016	0.000623	0.000010	0.049498	0.000136	0.866712	0.001345	99.98	46.99	306.34	±2.47
58.00W	0.000082	0.000005	0.000185	0.000011	0.000097	0.000002	0.005628	0.000031	0.101409	0.000082	99.30	5.34	301.26	±10.81
58.20W	0.000087	0.000003	0.000216	0.000013	0.000098	0.000006	0.005924	0.000034	0.108197	0.000237	98.00	5.62	302.26	±8.39
58.80W	0.000078	0.000002	0.000153	0.000011	0.000044	0.000002	0.001590	0.000016	0.032126	0.000126	100.00	1.50	306.22	±6.88
59.10W	0.000084	0.000004	0.000133	0.000016	0.000055	0.000003	0.002224	0.000020	0.042958	0.000089	96.64	2.10	295.24	±27.88
59.40W	0.000085	0.000007	0.000181	0.000010	0.000060	0.000002	0.003046	0.000014	0.057080	0.000076	96.68	2.88	294.78	±27.39
59.90W	0.000087	0.000005	0.000185	0.000006	0.000092	0.000005	0.005454	0.000027	0.097909	0.000108	97.58	5.17	295.09	±12.17
65.00W	0.000073	0.000005	0.000123	0.000009	0.000293	0.000007	0.022696	0.000099	0.398916	0.000311	100.00	21.54	305.77	±2.88

Results	40(r)/39(k)	±2σ	Age (Ma)	±2σ	MSWD	$^{39}Ar(k)$ (%,n)	K/Ca	±2σ
Weighted Plateau	17.3545	±0.1020 ±0.59%	305.22	±2.79 ±0.91%	0.92	100.00 9	0.511	±1.342
			External Error	±3.00	2.31	Statistical T Ratio		
			Analytical Error	±1.65	1.0000	Error Magnification		
Total Fusion Age	17.2895	±0.1220 ±0.71%	v304.17	±2.99 ±0.98%		9	17.786	±31.611
			External Error	±3.18				
			Analytical Error	±1.98				

displacement. A precise estimate of displacement is not available for this shear zone.

4.5. The Villalcampo Shear Zone (Gonzalez-Clavijo et al., 1993)

Sample IH-19 (41°31′28.61″N–6° 2′3.77″W) was taken from a coarse-grained quartz-feldspar S–C mylonite affecting the Ricobayo granodiorite (ca. 350 Ma, LA-ICPMS zircon U–Pb intrusion age, Gutiérrez-Alonso, unpublished data). The white mica grains that were picked for analysis were 600–1000 μm in diameter. Pervasive S–C structures and muscovite "mica fish" structures (Fig. 2) and local feldspar porphyroclasts indicate a dextral shear sense. This >2 km wide, 30 km long dextral shear zone strikes NW–SE, parallel to the main Variscan structural grain (Fig. 1B) and has been subjected to intense Permian hydrothermal alteration that produced episyenites and Au mineralizations (López-Moro et al., 2013). A minimum displacement of ~3.5 km has been established based on shear strain calculations (Gonzalez-Clavijo et al., 1993). The Villalcampo shear zone consists of muscovite-bearing phyllonites where it cuts metasedimentary rocks, and S–C proto- to ultra-mylonites where it involves granitoids, and was active under greenschist-facies conditions (Gonzalez-Clavijo et al., 1993).

5. Geochronological results

The results of $^{40}Ar/^{39}Ar$ dating are shown in Fig. 3 and Tables 1–5. The five muscovite samples yielded plateau ages ranging from 306 ± 3 to 310 ± 3 Ma (Kasimovian–Moscovian), with MSWD and P values ranging from 0.25 to 1.5 and 0.17 to 0.94 respectively. In all cases, the plateaus include more than 96% of ^{39}Ar released suggesting that the samples have not suffered any post-crystallization disturbance. All the ages are indistinguishable within error, indicating synchronicity of the activity of the five dated shear zones within ~3–4 million years, and suggesting a common origin for all of them. An estimate of the duration of the muscovite formation and/or recrystallization related shearing activity based on these five ages and assuming a gaussian distribution is

Table 5
Sample IH-19.
Same caption as in Table 1.

Laser intensity (%)	$^{36}Ar \pm 1\sigma$		$^{37}Ar \pm 1\sigma$		$^{38}Ar \pm 1\sigma$		$^{39}Ar \pm 1\sigma$		$^{40}Ar \pm 1\sigma$		$^{40}Ar^{*}$ (%)	$^{39}Ar_K$ (%)	Age $\pm 2\sigma$ (Ma)	
IH-19	J = 0.0106220 ± 0.0000425													
55.50W*	0.000095	0.000003	0.000171	0.000010	0.000034	0.000002	0.000776	0.000007	0.019034	0.000080	75.44	3.91	252.34	±86.22
56.00W	0.000087	0.000002	0.000159	0.000008	0.000042	0.000003	0.001144	0.000017	0.024911	0.000080	94.31	5.79	296.56	±54.76
56.30W	0.000079	0.000005	0.000215	0.000015	0.000154	0.000006	0.010726	0.000052	0.190087	0.000209	100.00	54.63	304.51	±3.12
56.40W	0.000078	0.000005	0.000139	0.000010	0.000034	0.000004	0.001136	0.000015	0.023896	0.000051	100.00	5.75	300.57	±8.05
56.50W	0.000083	0.000007	0.000184	0.000012	0.000033	0.000002	0.000541	0.000012	0.013712	0.000040	97.74	2.72	293.01	±161.04
57.20W	0.000073	0.000005	0.000145	0.000011	0.000030	0.000002	0.000673	0.000015	0.016257	0.000041	100.00	3.39	306.62	±13.62
57.20fW	0.000084	0.000005	0.000193	0.000006	0.000078	0.000006	0.004678	0.000015	0.085140	0.000165	100.00	23.81	303.30	±2.65

Results	40(r)/39(k)	±2σ	Age (Ma)	±2σ	MSWD	$^{39}Ar(k)$ (%,n)	K/Ca	±2σ
Weighted Plateau	17.2581	±0.1195 ±0.69%	303.66	±2.96 ±0.97%	0.25	96.09 6	1.603	±2.895
			External Error	±3.15	2.57	Statistical T Ratio		
			Analytical Error	±1.94	1.0000	Error Magnification		
Total Fusion Age	17.1110	±0.4065 ±2.38%	301.28	±6.96 ±2.31%		7	29.749	±141.73
			External Error	±7.04				
			Analytical Error	±6.59				

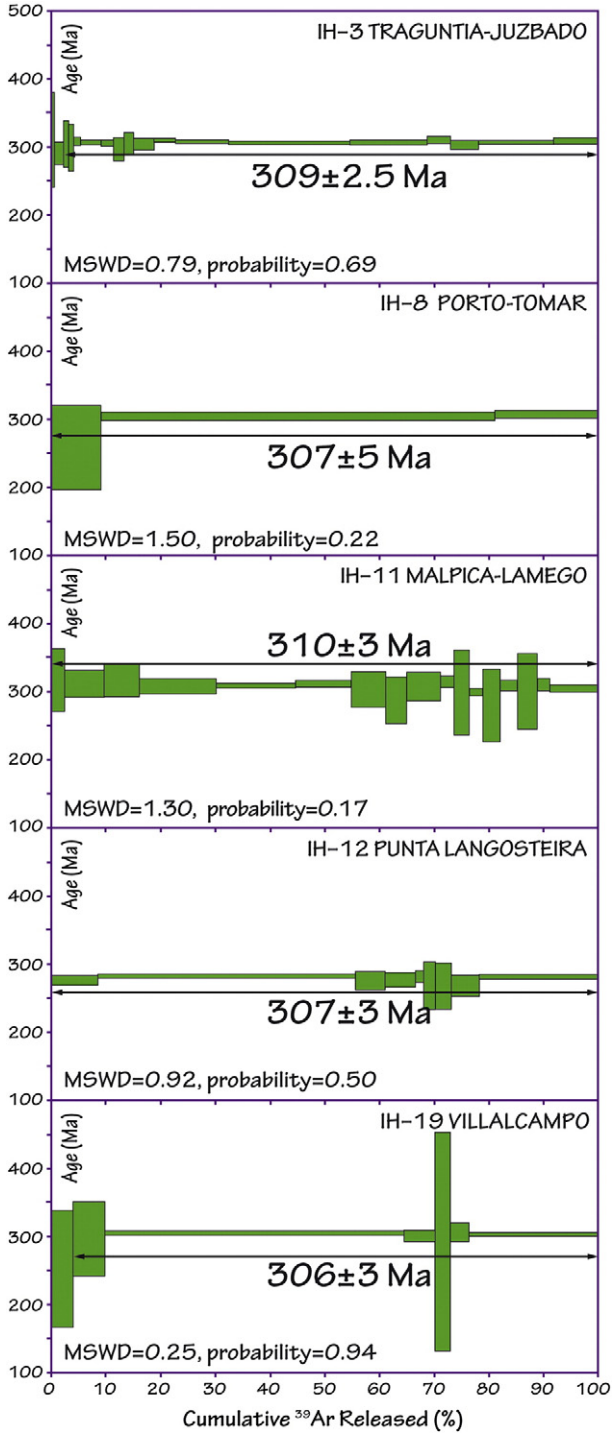

Fig. 3. $^{40}Ar/^{39}Ar$ geochronological results, represented as plateau diagrams, obtained for single-grain muscovite from of the strike–slip ductile shear zones studied in this work. All ages have been calculated using the decay constants of Renne et al. (2010) and include all source of uncertainties (see text for details).

given by the standard deviation of the population (±1.4 Ma) which suggests a maximum duration of ~2.8 Ma for muscovite formation conditions in all the studied shear zones. Assuming synchronicity of shearing, the best age estimate for shearing activity would be given by the weighted-mean of the five plateau ages: 308.3 ± 1.7 Ma (MSWD = 1.4; P = 0.22). This age is consistent with the inferred Moscovian age for the initial stages of oroclinal buckling based on paleomagnetic and structural studies (Weil et al., 2013).

6. Discussion

We have studied five mid-crustal ductile shear zones that are inferred to have accommodated vertical-axis rotations during orocline buckling (Gutiérrez-Alonso et al., 2008; Fig. 1). The present-day trace of exposed shear zones depicts in many cases (where the exposures are long enough) curved patterns that are consistent with active involvement in the oroclinal buckling. However, the spatial distribution and known displacements of existing shear zones do not accommodate the same amount of secondary rotation as the structural fabrics that formed prior to oroclinal buckling. These observations suggest that the large-scale shear zones that currently wrap around the Cantabrian Arc were activated during orocline buckling and played a role in accommodating lithospheric-scale orocline formation. Fig. 4 depicts our working hypothesis in which the ductile shear zones started to develop in the early stages of the orocline development following a strain pattern coherent with a tangential longitudinal strain dominated folding mechanism in the outer arc, in which extension paralleled the main fabric of the folded rocks (in our case, the trend of the main Variscan structures) and shortening was normal to it (Fig. 4B). Subsequent amplification of the fold would have led to the progressive change of orientation of the shear pattern, including bending the shear zone traces into their current curved outcrop pattern.

The main finding of this geochronological study is the synchronous development of a post-Variscan shear zone network at ca. 308 Ma that intensely modified the geometry of the main Variscan collisional architecture. The significance of the obtained ages is strengthened by the available $^{40}Ar/^{39}Ar$ age data from rocks not affected by the ductile shear zones; the non-sheared rocks invariably yield older ages than those obtained in this study (e.g. Dallmeyer et al., 1997; Gómez Barreiro et al., 2006; Rodriguez et al., 2003), indicating that the $^{40}Ar/^{39}Ar$ ages obtained within the shear zones do not record the cooling of the orogenic edifice but a subsequent deformation episode. This sequence of events is further constrained by granites that cut the shear zones and whose (zircon U–Pb) crystallization ages are between ca. 305 and 300 Ma (e.g. Valle Aguado et al., 2005; Gutiérrez-Alonso et al., 2011a,b; Costa, 2011). Given that the paleomagnetic and structural constraints place oroclinal development between ~310 and 299 Ma (Kollmeier et al., 2000; Pastor-Galán et al., 2011; Van der Voo et al., 1997; Weil et al., 2000, 2001, 2010, 2013), the obtained shearing ages are interpreted to reflect deformation during the early stages of orocline development. Subsequently, these ductile shear zones must have continued their activity in a more brittle fashion and in a cooler environment as exhumation and rapid erosion brought them closer to the surface leaving no isotopic record (in the Ar system) of their subsequent stages of development. The continuous activity of the studied shear zones until latest Carboniferous times is interpreted because some of the sampled shear zones affect the unconformably deposited continental Upper Pennsylvanian rocks in a brittle fashion (Chaminé et al., 2003; Dinis et al., 2012; Machado et al., 2012; Vázquez et al., 2007), although no geochronological record of this activity has been reported up to date. The sampled rocks should have been exposed at the surface, or very close to it, by ca. 305–303 Ma at least in some of the studied shear zones, and therefore they had to be exhumed to the surface by then. Exhumation is interpreted to have been driven by the lithospheric thinning causing thermal uplift in the outer part of the orocline according to the models proposed by Gutiérrez-Alonso et al. (2004) and the results of analogue modelling for orocline formation (Pastor-Galán et al., 2012b). The curved nature of the studied shear zones constitutes a further constraint on their development. Given the difficulty to generate curved shear zones with large associated displacements, we place their origin in the early stages of the orocline development as rather linear features that became progressively curved as the orocline curvature increased (Fig. 4).

The ages obtained in this study from syn-kinematic muscovite sampled in crustal-scale shear zones, together with similar ages obtained in

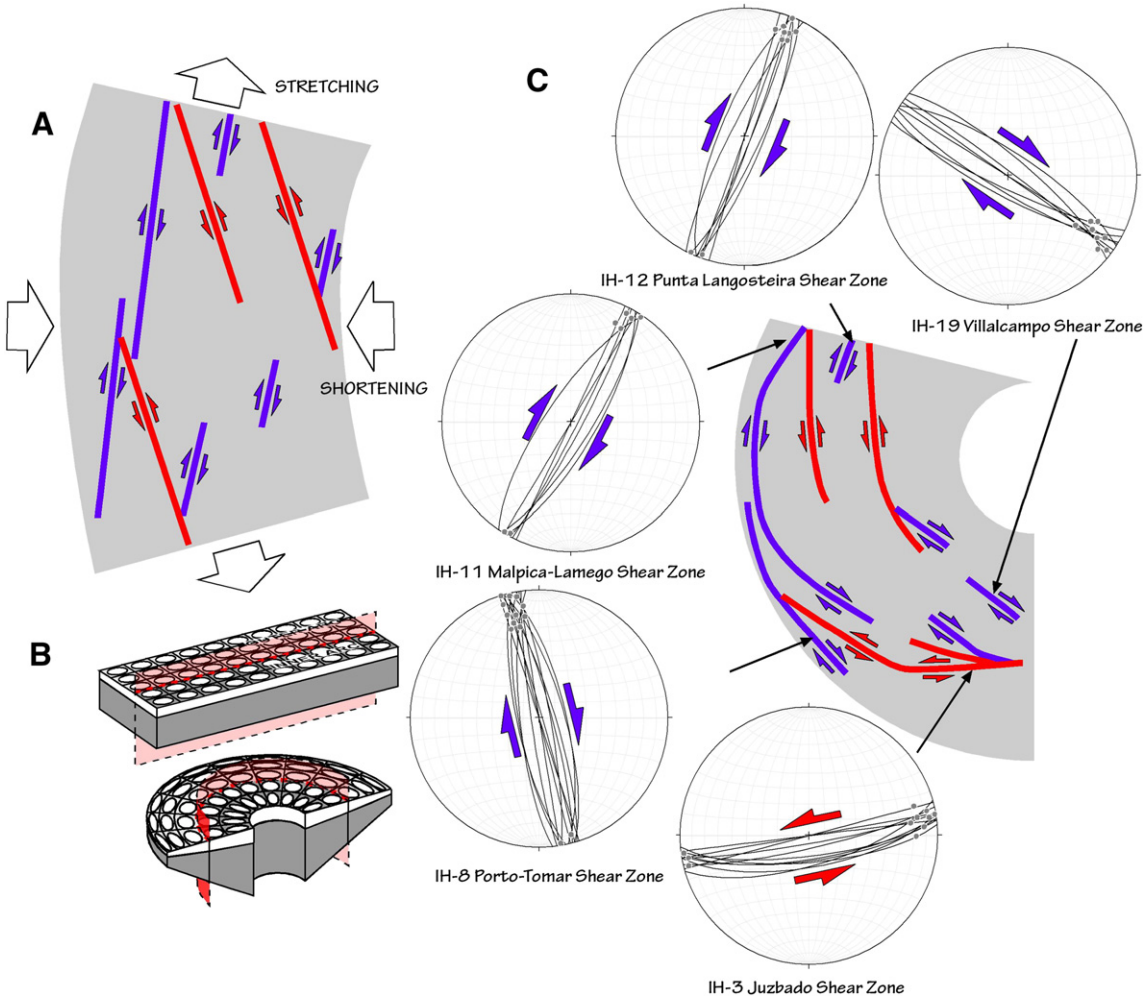

Fig. 4. A) Inferred initial disposition of the shear zone system during the onset of orocline development in NW Iberia. B) Schematic diagrams depicting the effect of lithospheric buckling around a vertical axis and the resultant strain field (modified tangential longitudinal strain). Strain ellipses depict arc-parallel shortening in the inner arc and arc-parallel stretching in the outer arc. The different behaviors of the mantle lithosphere in the inner and outer arcs and the increase in thickness of mantle lithosphere below the inner arc and thinning below the outer arc are highlighted. C) Present day disposition of the studied ductile shear zones, including stereonets (Wulff projection, lower hemisphere) of the orientation of the mylonitic foliation (lines) and the stretching lineation (dots) in the proximity of the sampling sites. Note the curved trace of the shear zones with respect to their initial disposition shown in A. B, modified from Gutiérrez-Alonso et al. (2004) and Ries and Shackleton (1976).

the WEVB (Ballèvre et al., 2009; Le Carlier de Veslud et al., 2013; Tartese et al., 2011; Turrillot et al., 2011) indicate that a major shear zone network helped shape the Cantabrian Arc. The nearly identical ages for the sampled shear zones along with their kinematic and geometric relationship to the larger Ibero-Armorican Arc, constrain their role in buckling of the Variscan orogen about a vertical axis of rotation and provide further evidence supporting the secondary nature of the orocline (cf. Weil et al., 2013). Penecontemporaneous activity of an orogen-scale shear-zone system coeval with formation of the Cantabrian Arc implies that the late- or post-Variscan evolution of Western Europe records major structures at all levels of the lithosphere related to oroclinal buckling of an originally linear mountain belt (Gutiérrez-Alonso et al., 2011a).

Previous hypotheses that explain the Cantabrian Arc-parallel shear zones as long-lived reactivated shear zones are not supported (but are not disproved by) our data. We conclude that the ductile shear zones were generated during late- to post-Variscan times in relation to the newly developed regional stress field that led to oroclinal bending.

In order to better illustrate the origin, nature and evolution of the shear zone system described in this paper, an animated illustration showing the formation of the orocline buckling process and the role of the studied shear zones can be obtained from Data Repository DR-1. In this animation, combined illustration of the shear zone ages and the orocline development demonstrates the time–space relationship between shear generation and the timing of the orocline. According to the available data, it is likely that, as explained above, the ages obtained reflect shear zone development during the initial stages of oroclinal buckling, prior to their exhumation and subsequent evolution in more brittle conditions.

Secondary orocline formation requires lithospheric-scale rotation around a vertical axis (Gutiérrez-Alonso et al., 2004, 2012; Johnston et al., 2013; Weil et al, 2013) and is likely to result in significant deformation at all structural levels. In the Cantabrian Arc, a record of oroclinal buckling has been obtained in the shallower structural levels through paleomagnetic studies (Weil et al., 2013) and by documentation of the sequential formation and rotation around a vertical-axis of structures developed before and during orocline development (Pastor-Galán et al., 2011, 2012a) and constrained to have started at ca. 310 Ma and completed by ca. 300 Ma. In addition, involvement of the lithospheric mantle and the lower crust, has been simulated through analogue modelling (Pastor-Galán et al., 2012b) and inferred from geochronological and isotopic studies (Fernandez-Suarez et al., 2006; Gutiérrez-Alonso et al., 2011a,b; Orejana et al., 2011). Seismic studies of similar syn-oroclinal

shear zones in northern Brittany have shown that these ductile shear zones transect the entire lithosphere (Vauchez and Tommasi, 2003). Documenting oroclinal bending at mid-crustal levels is difficult as the paleomagnetic record is non-existent and orocline related deformation is localized in discrete structures (or it reworks pre-existing ones). Where possible, constraining the timing of mid-crustal structures can help distinguish between pre- and syn-oroclinal structures, as is the case in Western Europe. Large vertical strike–slip shear zones are expected structures in oroclines, as such structures are necessary to accommodate vertical axis buckling, especially in the outer arc. The study of the geometry and timing of such structures in other curved mountain belts is required to better understand their nature, origin and evolution.

7. Conclusions

Ages obtained from 5 large scale shear zones in western Iberia provide coeval ages that cluster around 308 Ma. Given that the obtained ages are within the time interval in which the Cantabrian–Ibero-Armorican Arc was developed, we interpret that both processes are linked, the shear zone formation being a necessary effect of the lithospheric-scale accommodation of deformation during oroclinal buckling. These shear zones are not likely to have been active prior or during the building of the main orogenic edifice.

Supplementary data to this article can be found online at http://dx.doi.org/10.1016/j.tecto.2014.12.009.

Acknowledgements

The financial support of GG-A, DP-G and ABW was supplied by Research Project ODRE III (Oroclines and Delamination: Relations and Effects) CGL2013-46061 from the Spanish Ministry of Economy and Competitiveness. ASC contribution forms TRaX Record #320 and is supported by ARC grant FT120100340. JFS acknowledges the financial support from project CGL201234618 from the Spanish Ministry of Economy. STJ acknowledges NSERC for a Discovery Grant (RGPIN-2014-06533). This paper is part of UNESCO IGCP Projects 574: Buckling and Bent Orogens, and Continental Ribbons and 597: Amalgamation and breakup of Pangaea: The Type Example of the Supercontinent Cycle. Constructive reviews of a previous version of this paper by G. Lister and journal reviews by J.K. Lee and M.F. Pereira are kindly acknowledged.

References

Aerden, D.G.A.M., 2004. Correlating deformation in Variscan NW-Iberia using porphyroblasts; implications for the Ibero-Armorican arc. J. Struct. Geol. 26, 177–196.
Aguado, B.V., Azevedo, M.R., Schaltegger, U., Catálan, J.R.M., Nolan, J., 2005. U–Pb zircon and monazite geochronology of Variscan magmatism related to syn-convergence extension in Central Northern Portugal. Lithos 82, 169–184.
Arenas, R., Martínez Catalán, J.R., 2003. Low-P metamorphism following a Barrovian-type evolution. Complex tectonic controls for a common transition, as deduced in the Mondoñedo thrust sheet (NW Iberian Massif). Tectonophysics 365, 143–164.
Argand, E., 1924. La tectonique de L'Asie. 13th International Geological Congress: Brusselspp. 171–372.
Arthaud, F., Matte, P., 1977. Late Paleozoic strike–slip faulting in southern Europe and northern Africa — results of a right-lateral shear zone between Appalachians and Urals. Geol. Soc. Am. Bull. 88, 1305–1320.
Ballèvre, M., Bosse, V., Ducassou, C., Pitra, P., 2009. Palaeozoic history of the Armorican Massif: models for the tectonic evolution of the suture zones. C. R. Geosci. 341, 174–201.
Bard, J.P., Capdevila, R., Matte, P., 1968. La Structure de la Chaine Hercynienne de la Meseta Iberique. Comparison avec les Segments Voisins: Paris, Editions Technip.
Brun, J.P., Burg, J.P., 1982. Combined thrusting and wrenching in the Ibero-Armorican Arc — a corner effect during continental collision. Earth Planet. Sci. Lett. vol. 61, 319–332.
Buck, W.R., Martinez, F., Steckler, M., Cochran, J.R., 1988. Thermal consequences of lithospheric extension: pure and simple. Tectonics vol. 7, 213–234.
Carey, S.W., 1955. The orocline concept in geotectonics. Proc. R. Soc. Tasmania 89, 255–288.
Le Carlier de Veslud, Ch., Alexander, P., Ruffet, G., Cuney, M., Cheilletz, A., 2013. A two-stage exhumation in Western French Massif Central: new geochronological evidences of syn-collisional extension. Lithos 175–176, 1–15.
Cepedal, A., Fuertes-Fuente, M., Martín-Izard, A., García-Nieto, J., Boiron, M.C., 2013. An intrusion-related gold deposit (IRGD) in the NW of Spain, the Linares deposit: igneous rocks, veins and related alterations, ore features and fluids involved. J. Geochem. Explor. 124, 101–126.
Chaminé, H.I., Gama Pereira, L.C., Fonseca, P.E., Moço, L.P., Fernanades, J.P., Rocha, F.T., Flores, D., Pinto de Jesus, A., Gomes, C., Soares de Andrade, A.A., Araújo, A., 2003. Tectonostratigraphy of Middle and Upper Palaeozoic black shales from the Porto-Tomar-Ferreira do Alentejo shear zone (W Portugal): new perspectives on the Iberian Massif. Geobios 36, 649–663.
Costa, M.M., 2011. Geoquimica dos granitoides de aguiar da Beira, Norte de Portugal. Universidade de Aveiro (Unpublished PhD thesis).
Costa, M.M., Neiva, A.M.R., Azevedo, M.R., Corfu, F., 2014. Distinct sources for syntectonic Variscan granitoids: insights from the Aguiar da Beira region, Central Portugal. Lithos 196–197, 83–98.
Dallmeyer, R.D., Catalan, J.R.M., Arenas, R., Ibarguchi, J.I.G., Alonso, G.G., Farias, P., Bastida, F., Aller, J., 1997. Diachronous Variscan tectonothermal activity in the NW Iberian Massif: evidence from Ar-40/Ar-39 dating of regional fabrics. Tectonophysics 277, 307–337.
Dias, R., Ribeiro, A., 1995. The Ibero-Armorican Arc: a collision effect against an irregular continent? Tectonophysics 113–128.
Díaz García, F., 1990. La Geología del sector Occidental del Complejo de Ordenes (Cordillera Hercynica, NW de España). Nova Terra, 3. Ediciones O Castro, A Coruña (269 pp.).
Díez Balda, M.A., Martínez Catalán, J.R., Ayarza Arribas, P., 1995. Syn-collisional extensional collapse parallel to the orogenic trend in a domain of steep tectonics: the Salamanca Detachment Zone (Central Iberian Zone, Spain). J. Struct. Geol. 17, 163–182.
Díez Fernández, R., Martínez Catalán, J.R., Arenas, R., Abati, J., 2011. Tectonic evolution of a continental subduction-exhumation channel: Variscan structure of the basal allochthonous units in NW Spain. Tectonics 30, TC3009.
Dinis, P., Anderson, T., Machado, G., Guimaraes, F., 2012. Detrital zircon U–Pb ages of a late-Variscan Carboniferous succession associated with the Porto-Tomar shear zone (West Portugal): provenance implications. Sediment. Geol. 273–274, 19–29.
Fernández Suárez, J., 1994. Petrología de los granitos peralumínicos y metamorfismo de la banda Boal-Los Ancares. PhD Thesis. Departamento de Geología, Univ. de Oviedo, pp. 1–418.
Fernández-Suárez, J., Dunning, G.R., Jenner, G.A., Gutiérrez-Alonso, G., 2000. Variscan collisional magmatism and deformation in NW Iberia: constraints from U–Pb geochronology of granitoids. J. Geol. Soc. vol. 157, 565–576.
Fernandez-Suarez, J., Arenas, R., Jeffries, T.E., Whitehouse, M.J., Villaseca, C., 2006. A U–Pb study of zircons from a lower crustal granulite xenolith of the Spanish central system: a record of Iberian lithospheric evolution from the Neoproterozoic to the Triassic. J. Geol. 114, 471–483.
Gómez Barreiro, J., Wijbrans, J., Castiñeiras, P., Martínez Catalán, J.R., Arenas, R., Díaz García, F., Abati, J., 2006. $^{40}Ar/^{39}Ar$ laserprobe dating of mylonitic fabrics in a polyorogenic terrane of NW Iberia. J. Geol. Soc. Lond. 163, 61–73.
González-Clavijo, E., 1990. Estudio geométrico y cinemático de la cizalla de Villalcampo (Zamora). Aplicacion a la prospeción minera (MSc Thesis, Univ Salamanca: 98 pp.).
Gonzalez-Clavijo, E., Diez Balda, M.A., Alvarez, F., 1993. Structural study of a semiductile strike–slip system in the Central Iberian Zone (Variscan Fold Belt, Spain) — structural controls on gold deposits. Geol. Rundsch. 82, 448–460.
Gutiérrez-Alonso, G., Fernández-Suárez, J., Weil, A.B., 2004. Orocline triggered lithospheric delamination. Geol. Soc. Am. Spec. Pap. 383, 121–131.
Gutiérrez-Alonso, G., Fernandez-Suarez, J., Weil, A.B., Murphy, J.B., Nance, R.D., Corfu, F., Johnston, S.T., 2008. Self-subduction of the Pangaean global plate. Nat. Geosci. 1, 549–553.
Gutiérrez-Alonso, G., Fernández-Suárez, J., Jeffries, T.E., Johnston, S.T., Pastor-Galán, D., Murphy, J.B., Franco, M.P., Gonzalo, J.C., 2011a. Diachronous post-orogenic magmatism within a developing orocline in Iberia, European Variscides. Tectonics 30, TC5008.
Gutiérrez-Alonso, G., Murphy, B., Fernández-Suárez, J., Weil, A.B., Franco, M.P., Gonzalo, J.C., 2011b. Lithospheric delamination in the core of Pangea: Sm–Nd insights from the Iberian mantle. Geology 155–158.
Gutiérrez-Alonso, G., Johnston, S.T., Weil, A.B., Pastor-Galán, D., Fernández-Suárez, J., 2012. Buckling an orogen: the Cantabrian Orocline. GSA Today 22 (7), 4–9.
Iglesias, M., Ribeiro, A., 1981. La zone de cisaillement ductile de Juzbado (Salamanca)-Penalva do Castelo (Viseu): Un linéament ancien reactivé pendant l'orogenese Hercynienne? 67. Comunicações dos Serviços Geológicos de Portugal
Johnston, S.T., Weil, A.B., Gutiérrez-Alonso, G., 2013. Oroclines: thick and thin. GSA Bull. http://dx.doi.org/10.1130/B30765.1.
Jourdan, F., Renne, P.R., 2007. Age calibration of the Fish Canyon sanidine $^{40}Ar/^{39}Ar$ dating standard using primary K–Ar standards. Geochim. Cosmochim. Acta 71, 387–402.
Jourdan, F., Verati, C., Feraud, G., 2006. Intercalibration of the Hb3gr $^{40}Ar/^{39}Ar$ dating standard. Chem. Geol. 231, 177–189.
Kollmeier, J.M., van der Pluijm, B.A., Van der Voo, R., 2000. Analysis of Variscan dynamics; early buckling of the Cantabria-Asturias Arc, northern Spain. Earth Planet. Sci. Lett. 181, 203–216.
Koppers, A.A.P., 2002. ArArCALC-software for $^{40}Ar/^{39}Ar$ age calculations. Comput. Geosci. 28, 605–619.
Kröner, U., Romer, R.L., 2013. Two plates–many subduction zones: the Variscan orogeny reconsidered. Gondwana Res. 24, 298–329.
Lister, G.S., Snoke, A.W., 1984. S–C mylonites. J. Struct. Geol. 6, 617–638.
Llana-Funez, S., Marcos, A., 2001. The Malpica–Lamego line: a major crustal-scale shear zone in the Variscan belt of Iberia. J. Struct. Geol. 23, 1015–1030.
López-Moro, F.J., Moro, M.C., Timón, S.M., Cembranos, M.L., Cózar, J., 2013. Constraints regarding gold deposition in episyenites: the Permian episyenites associated with the Villalcampo Shear Zone, central western Spain. Int. J. Earth Sci. 102, 721–744.

G. Machado, I. Dias da Silva, P. Almeida, Palynology, 2012. Stratigraphy and geometry of the Pennsylvanian continental Santa Susana Basin (SW Portugal), J. Iber. Geol. 38 (2) 429–448.
Maffione, M., Speranza, F., Faccena, C., 2009. Bending of the Bolivian orocline and growth of the central Andean plateau: paleomagnetic and structural constraints from the Eastern Cordillera (22–24S, NW Argentina). Tectonics 28, TC4006.
Maffione, M., Speranza, F., Faccenna, C., Rossello, E., 2010. Paleomagnetic evidence for a pre-early Eocene (~50 Ma) bending of the Patagonian orocline (Tierra del Fuego, Argentina): paleogeographic and tectonic implications. Earth Planet. Sci. Lett. 289, 273–286.
Maffione, M., Speranza, F., Cascella, A., Longhitano, S.G., Chiarella, D., 2013. A ~125° post-early Serravallian counterclockwise rotation of the Gorgoglione Formation (Southern Apennines, Italy): new constraints for the formation of the Calabrian Arc. Tectonophysics 590, 24–37.
Marques, F.O., Mateus, A., Tassinari, C., 2002. The Late-Variscan fault network in central-northern Portugal (NW Iberia): a re-evaluation. Tectonophysics 359, 255–270.
Marshak, S., 2004. Arcs, oroclines, salients, and syntaxes — the origin of map-view curvature in fold-thrust belts. In: McClay, K.R. (Ed.), Thrust Tectonics and Petroleum Systems 82. American Association of Petroleum Geologists Memoir, pp. 131–156.
Martínez Catalán, J.R., Arenas, R., Díaz García, F., Gómez-Barreiro, J., González Cuadra, P., Abati, J., Castiñeiras, P., Fernández-Suárez, J., Sánchez Martínez, S., Andonaegui, P., González Clavijo, E., Díez Montes, A., Rubio Pascual, F.J., Valle Aguado, B., 2007. Space and time in the tectonic evolution of the northwestern Iberian Massif. Implications for the comprehension of the Variscan belt. In: Hatcher Jr., R.D., Carlson, M.P., McBride, J.H., Martínez Catalán, J.R. (Eds.), 4-D Framework of Continental Crust, Volume 200: Memoir: Boulder, Geological Society of America.
F.J. Martínez, J. Rolet, 1988. Late Paleozoic metamorphism in the Northwestern Iberian peninsula, Brittany and related areas in southwest Europe, In: The Caledonian–Appalachian Orogen: Geol. Soc. Spec. Pub., Blackwell Scientific Publications, London, pp. 611–620.
Martínez-Catalán, J.R., 1990. A non-cylindrical model for the northwest Iberian allochthonous terranes and their equivalents in the Hercynian belt of Western Europe. Tectonophysics 179, 253–272.
Martínez-Catalán, J.R., 2011. Are the oroclines of the Variscan belt related to late Variscan strike–slip tectonics? Terra Nova 00, 1–7.
Martínez-Catalán, J.R., 2012. The Central Iberian arc, an orocline centered in the Iberian Massif and some implications for the Variscan belt. Int. J. Earth Sci. 101, 1299–1314.
Martínez-García, E., 2013. An Alleghenian orocline: the Asturian Arc, northwestern Spain. Int. Geol. Rev. 55, 367–381.
Martín-Izard, A., Fuertes-Fuente, M., Cepedal, A., Moreiras, D., García-Nieto, J., Maldonado, C., Pevida, L.R., 2000. The Río Narcea gold belt intrusions: geology, petrology, geochemistry and timing. J. Geochem. Explor. 71, 103–117.
Martín-Izard, A., Gumiel, P., Arias, M., Cepedal, A., Fuertes-Fuente, M., Reguilón, R., 2009. Genesis and evolution of the structurally controlled vein mineralization (Sb–Hg) in the Escarlati deposit (León, Spain): evidence from fault population analysis methods, fluid-inclusion research and stable isotope data. J. Geochem. Explor. 100, 51–66.
Martins., C.B.H., Sant'Ovaia, H., Abreu, J., Oliveira, M., Noronha, F., 2011. Emplacement of the Lavadores granite (NW Portugal): U/Pb and AMS results. Compt. Rendus Geosci. 343, 387–396.
Orejana, D., Villaseca, C., Armstrong, R.A., Jeffries, T.E., 2011. Geochronology and trace element chemistry of zircon and garnet from granulite xenoliths: constraints on the tectonothermal evolution of the lower crust under central Spain. Lithos 124, 103–116.
Orejana, D., Villaseca, C., Valverde-Vaquero, P., Belousova, E.A., Armstrong, R.A., 2012. U–Pb geochronology and zircon composition of late Variscan S- and I-type granitoids from the Spanish Central System batholith. Int. J. Earth Sci. 101, 1789–1815.
Pastor-Galán, D., Gutierréz-Alonso, G., Weil, A.B., 2011. Orocline timing through joint analysis: insights from the Ibero-Armorican Arc. Tectonophysics 507, 31–46.
Pastor-Galán, D., Gutiérrez-Alonso, G., Mulchrone, K.F., Huerta, P., 2012a. Conical folding in the core of an orocline. A geometric analysis from the Cantabrian Arc (Variscan Belt of NW Iberia). J. Struct. Geol. 39, 2010–2223. http://dx.doi.org/10.1016/j.jsg.2012.02.010.
Pastor-Galán, D., Gutiérrez-Alonso, G., Zulauf, G., Zanella, F., 2012b. Analogue modeling of lithospheric scale orocline buckling: constraints on the evolution of the Ibero Armorican Arc. Geol. Soc. Am. Bull. 124, 1293–1309.
Pereira, M.F., Chichorro, M., Williams, I.S., Silva, J.B., Fernández, C., Díaz-Azpiroz, M., Apraiz, A., Castro, A., 2009. Variscan intra-orogenic extensional tectonics in the Ossa–Morena Zone (Évora–Aracena–Lora del Rio metamorphic belt, SW Iberian Massif): SHRIMP zircon U–Th–Pb geochronology. In: Murphy, J.B., Keppie, J.D., Hynes, A.J. (Eds.), Ancient Orogens and Modern Analogues. 327. Geological Society, London, pp. 215–237 (Special Publications).
Pereira, M.F., Silva, J.B., Drost, K., Chichorro, M., Apraiz, A., 2010. Relative timing of transcurent displacements in northern Gondwana: U–Pb laser ablation ICP-MS zircon and monazite geochronology of gneisses and sheared granites from the western Iberian Massif (Portugal). Gondwana Res. 17, 461–481.
Pereira, M.F., Chichorro, M., Silva, J.B., Ordóñez-Casado, B., Lee, J.K.W., Williams, I.S., 2012. Early carboniferous wrenching, exhumation of high-grade metamorphic rocks and basin instability in SW Iberia: constraints derived from structural geology and U–Pb and ^{40}Ar–^{39}Ar geochronology. Tectonophysics 558–559, 28–44.
Pereira, M.F., Castro, A., Fernández, C., 2015. The inception of a Paleotethyian magmatic arc in Iberia. Geosci. Front. http://dx.doi.org/10.1016/j.gsf.2014.02.006 (in press).
Ponce de Leon, M.I., Choukroune, P., 1980. Shear zones in the Iberian Arc. J. Struct. Geol. 2, 63–68.
Regencio Macedo, C.A., 1988. Granitoides, Complexo Xisto-Graiváquico e Ordovícico na regiao entre Trancoso e Pinhel (Portugal Central): geologia, petrologia, geocronologia. Universidade de Coimbra, Coimbra.
Renne, P.R., Mundil, R., Balco, G., Min, K., Ludwig, K.R., 2010. Joint determination of ^{40}K decay constants and ^{40}Ar/^{40}K for the Fish Canyon sanidine standard, and improved accuracy for ^{40}Ar/^{39}Ar geochronology. Geochim. Cosmochim. Acta 74 (18), 5349–5367. http://dx.doi.org/10.1016/j.gca.2010.06.017.
Ribeiro, A., Pereira, E., Severo, L., 1980. Análise da deformaçao da zona de cisalhamento Porto-Tomar na transversal de Oliveira de Aeméis. Comunicaçoes dos Serviços Geológicos de Portugal vol. 66, pp. 3–9.
Ribeiro, A., Munha, J., Dias, R., Mateus, A., Pereira, E., Ribeiro, L., Fonseca, P., Araujo, A., Oliveira, T., Romao, J., Chamine, H., Coke, C., Pedro, J., 2007. Geodynamic evolution of the SW Europe Variscides. Tectonics 26, 24.
Ries, A.C., Shackleton, R.M., 1976. Patterns of strain variation in arcuate fold belts. Philos. Trans. R. Soc. Lond. A Math. Phys. Sci. 283, 281–288.
Rodriguez, J., Cosca, M.A., Ibarguchi, J.I.G., Dallmeyer, R.D., 2003. Strain partitioning and preservation of Ar-40/Ar-39 ages during Variscan exhumation of a subducted crust (Malpica–Tui complex, NW Spain). Lithos 70, 111–139.
Rosenbaum, G., Li, P., Rubatto, D., 2012. The contorted New England Orogen (eastern Australia): new evidence from U–Pb geochronology of early Permian granitoids. Tectonics 31 TC1006.
Şengör, A.M.C., 2013. The Pyrenean Hercynian Keirogen and the Cantabrian Orocline as genetically coupled structures. J. Geodyn. 65, 3–21.
Shaw, J., Johnston, S.T., Gutiérrez-Alonso, G., Weil, A.B., 2012. Oroclines of the Variscan orogen of Iberia: paleocurrent analysis and paleogeographic implications. Earth Planet. Sci. Lett. 329–330, 60–70.
Shelley, D., Bossiere, G., 2000. A new model for the Hercynian Orogen of Gondwanan France and Iberia. J. Struct. Geol. 22, 757–776.
Shelley, D., Bossière, G., 2002. Megadisplacements and the Hercynian orogen of Gondwanan France and Iberia. In: Martínez Catalán, J.R., Hatcher Jr., R.D., Arenas, R., Díaz García, F. (Eds.), Variscan–Appalachian Dynamics: The Building of the Late Paleozoic Basement: Boulder Colorado. Geological Society of America Special Paper 364, pp. 209–222.
Simancas, J.F., Tahiri, A., Azor, A., Lodeiro, F.G., Poyatos, D.J.M., El Hadi, H., 2005. The tectonic frame of the Variscan–Alleghanian orogen in southern Europe and northern Africa. Tectonophysics 398, 181–198.
Simancas, J.F., Ayarza, P., Azor, A., Carbonell, R., Martínez Poyatos, D., Pérez-Estaún, A., González-Lodeiro, F., 2013. A seismic geotraverse across the Iberian Variscides: orogenic shortening, collisional magmatism and orocline development. Tectonics http://dx.doi.org/10.1002/tect.20035.
Steiger, R.H., Jäger, E., 1977. Subcommission on geochronology: convention on the use of decay constants in geo- and cosmochronology. Earth Planet. Sci. Lett. 36, 359–362.
Tartese, R., Poujol, M., Ruffet, G., Boulvais, P., Yamato, P., Kosler, J., 2011. New U–Pb zircon and ^{40}Ar/^{39}Ar muscovite age constraints on the emplacement of the Lizio syntectonic granite (Armorican Massif, France). Compt. Rendus Geosci. 343, 443–453.
Turrillot, P., Augier, R., Monié, P., Faure, M., 2011. Late orogenic exhumation of the Variscan high-grade units (South Armorican Domain, western France), combined structural and ^{40}Ar/^{39}Ar constraints. Tectonics 30, TC5007.
Valverde-Vaquero, P., Díez-Balda, M.A., Díez-Montes, A., Dörr, W., Escuder-Viruete, J., Gonzalez-Clavijo, E., Malusk, i H., Rodríguez-Fernández, L.R., Rubio, F., Villar, P., 2007. The "hot orogen": two separate Variscan low-pressure metamorphic events in the Central Iberian zone. 2007. Geolgie de la France, p. 168.
Van der Voo, R., 2004. Paleomagnetism, oroclines, and growth of the continental crust. GSA Today 14, 4–9.
Van der Voo, R., Stamatakos, J.A., Parés, J.M., 1997. Kinematic constraints on thrust-belt curvature from syndeformational magnetizations in the Lagos del Valle Syncline in the Cantabrian Arc Spain. J. Geophys. Res. 102, 10,105–10,119. http://dx.doi.org/10.1029/97JB00263.
Vauchez, A., Tommasi, A., 2003. Wrench faults down to the asthenosphere: geological and geophysical evidence and thermo-mechanical effects. In: Storti, F., Holdsworth, R.E., Salvini, F. (Eds.), Intraplate Strike–Slip Deformation Belts. 210. Geological Society of London, London, pp. 15–34 (Special Publication).
Vázquez, M., Abad, I., Jiménez-Millán, J., Rocha, F.T., Fonseca, P.E., Chaminé, H.I., 2007. Prograde epizonal clay mineral assemblages and retrograde alteration in tectonic basins controlled by major strike–slip zones (W Iberian Variscan chain). Clay Miner. 42, 109–128.
Villar Alonso, P., Escuder Viruete, J., Martínez Catalán, J.R., 1992. La Zona de Cizalla de Juzbado-Penalva do Castelo en el Sector Español. III congreso Geológico de España y VIII Latinoamericano de Geología. Volume Simposios, 2: Salamanca, pp. 446–456.
Weil, A.B., Sussman, A.J., 2004. Classifying curved orogens based on timing relationships between structural development and vertical-axis rotations. In: Sussman, A.J., Weil, A.B. (Eds.), Orogenic Curvature: Integrating Paleomagnetic and Structural Analyses Vol. 383. Geological Society of America, pp. 1–16.
Weil, A.B., Van der Voo, R., van der Pluijm, B., Parés, J.M., 2000. The formation of an orocline by multiphased deformation: a paleomagnetic investigation of the Cantabria–Asturias Arc Hinge-Zone (northern Spain). J. Struct. Geol. 22, 735–756.
Weil, A.B., van der Voo, R., van der Pluijm, B.A., 2001. Oroclinal bending and evidence against the Pangea megashear: the Cantabria–Asturias arc (northern Spain). Geology vol. 2 (9), 991–994.
Weil, A., Gutiérrez-Alonso, G., Conan, J., 2010. New time constraints on lithospheric-scale oroclinal bending of the Ibero-Armorican Arc: a palaeomagnetic study of earliest Permian rocks from Iberia. J. Geol. Soc. Lond. vol. 167, 127–143.
Weil, A., Gutiérrez-Alonso, G., Johnston, S.T., Pastor-Galán, D., 2013. Kinematic constraints on buckling a lithospheric-scale orocline along the northern margin of Gondwana: a geologic synthesis. Tectonophysics 582, 25–49.